

THE FATE OF DEAD RADIO-LOUD ACTIVE GALACTIC NUCLEI: A
NEW PREDICTION OF LONG-LIVED SHELL EMISSIONHIROTAKA ITO¹, MOTOKI KINO², NOZOMU KAWAKATU³, MONICA ORIENTI⁴*draft version March 2, 2024,*

ABSTRACT

We examine the fate of a dead radio source in which jet injection from the central engine has stopped at an early stage of its evolution ($t = t_j \lesssim 10^5$ yr). To this aim, we theoretically evaluate the evolution of the emission from both the lobe and the shell, which are composed of shocked jet matter and a shocked ambient medium (i.e., shell), respectively. Based on a simple dynamical model of expanding lobe and shell, we clarify how the broadband spectrum of each component evolves before and after the cessation of the jet activity. It is shown that the spectrum is strongly dominated by the lobe emission while the jet is active ($t \leq t_j$). On the other hand, once the jet activity has ceased ($t > t_j$), the lobe emission fades out rapidly, since fresh electrons are no longer supplied from the jet. Meanwhile, shell emission only shows a gradual decrease, since fresh electrons are continuously supplied from the bow shock that is propagating into the ambient medium. As a result, overall emission from the shell overwhelms that from the lobe at wide range of frequencies from radio up to gamma-ray soon after the jet activity has ceased. Our result predicts a new class of dead radio sources that are dominated by shell emission. We suggest that the emission from the shell can be probed in particular at a radio wavelengths with the Square Kilometer Array (SKA) phase 1.

Subject headings: particle acceleration — radiation mechanisms: non-thermal — galaxies: active — galaxies: jets —

1. INTRODUCTION

Relativistic jets in radio-loud active galactic nuclei (AGNs) dissipate their kinetic energy via interactions with surrounding interstellar medium (ISM) or intracluster medium (ICM), and inflate a bubble composed of decelerated jet matter, which is often referred to as cocoon (e.g., Begelman et al. 1984, for review). Since the cocoon is highly overpressured against the ambient ISM/ICM (Begelman & Cioffi 1989), bow shock is driven into the ambient matter. As a result, the shocked ambient gas forms a thin shell around the cocoon and envelopes the whole system. The thin shell structure persists until the cocoon pressure decreases and the pressure equilibrium is eventually achieved (Reynolds et al. 2001).

The dissipation of jet energy due to the interaction with the ambient matter is accompanied by particle acceleration and non-thermal electrons are supplied to the cocoon from the jet. It is well established that prominent radio emission is produced by the accelerated electrons within the cocoon via synchrotron radiation. Hence, the cocoon is often termed as radio lobe. Inverse Compton (IC) emission by the same population of electrons is sometimes observed at higher frequencies such as X-ray (e.g., Hardcastle et al. 2002; Isobe et al. 2002; Croston et al. 2005; Kataoka & Stawarz 2005) and, in some cases, even at gamma-rays (Abdo et al. 2010).

As in the case of the lobe, shell is also expected to give

rise to non-thermal emission, since the bow shock offers a site of particle acceleration (Fujita et al. 2007; Berezhko 2008; Bordas et al. 2011; Ito et al. 2011; Kino et al. 2013). Observationally, however, detection of shell emission is rare and reported only at X-ray energies (Kraft et al. 2003; Croston et al. 2007; Jetha et al. 2008). Moreover, most of them are thermal origin, and only one source, the most nearby radio galaxy Centaurus A, shows evidence for the non-thermal emission at X-ray (Croston et al. 2009). Due to the lack of observations, the number of studies that focus on the shell emission is small and, therefore, its nature is poorly known.

To tackle this issue, we have explored the evolution of the emission from both the lobe and shell simultaneously in the previous studies (Ito et al. 2011; Kino et al. 2013). Under the assumption that the jet is active throughout the evolution, it is shown that the overall spectrum is strongly overwhelmed by the lobe emission at most of the frequencies. Hence, detection of the shell emission is likely to be hampered by the lobe emission and limited in a narrow range of frequencies. This provides a natural explanation on the reason why the detection of shell is rare.

While the large contrast between the lobe and shell emission is expected to be maintained as long as the jet continuously injects energy into the lobe, the situation may change drastically after the jet activity has ceased. It is known from the literature (e.g., Komissarov & Gubanov 1994; Nath 2010; Mocz et al. 2011) that luminosity of the lobe emission shows a rapid decrease when the jet activity is stopped. This is because the radiative cooling leads to the depletion of non-thermal electrons, since fresh electrons are no longer supplied from the jet. Therefore, it is often claimed that these dead sources simply fade out soon after the jet activity ceases. How-

hirotaka.ito@riken.jp

¹ Astrophysical Big Bang Laboratory, RIKEN, Saitama 351-0198, Japan² Korea Astronomy and Space Science Institute, 776 Daedukdae-ro, Yuseong-gu, Daejeon 305-348, Korea³ National Institute of Technology, Kure, 2-2-11 Agaminami, Kure, Hiroshima, 737-8506, Japan⁴ INAF Istituto di Radioastronomia, via Gobetti 101, I-40129 Bologna, Italy

ever, the above statement may not be true when contribution from the shell emission is considered. Since the bow shock propagating into the ambient medium is active even after the jet activity has ceased, it continues to supply fresh electrons in the shell (Reynolds & Begelman 1997; Reynolds et al. 2002; Perucho et al. 2011). As a result, emission from the shell can persist its luminosity and eventually dominates over that from the lobe. However, up to present, there are no quantitative studies that focus on this issue.

Regarding the evolutionarily track of radio sources, it is widely accepted that young compact radio sources, i.e., Gigahertz Peaked Spectrum (GPS) and Compact Steep Spectrum (CSS) sources, represent the young stage ($\sim 10^3 - 10^5$ yr; e.g., O’Dea 1998) of typical well-extended classical radio galaxies that have estimated ages of $\sim 10^7 - 10^8$ yr. On the other hand, it is not clear whether “all” compact radio sources can survive to the ages of typical radio galaxies. This comes from observational fact that these compact sources represent a large fraction ($\sim 15 - 30\%$) in the flux-limited catalogue of the radio sources (Fanti et al. 1995), which is much larger than the expected value ($\lesssim 0.1\%$) from their youthness. A simple and plausible explanation for this discrepancy is that significant fraction of young compact radio sources stop their jet activity at an early stage of their evolution ($\lesssim 10^5$ yr) (Alexander 2000; Marecki et al. 2003; Gugliucci et al. 2005; Orienti & Dallacasa 2010; Orienti et al. 2010; Kunert-Bajraszewska et al. 2010). Then, large population of compact dead radio sources in which jet injection from central engine has ceased is expected to be hidden in the universe. Therefore, clarifying the evolution of dead radio sources including the contribution of shell is essential for revealing the evolution of radio sources.

Motivated by these backgrounds, we explore the emission from radio sources in which jet activity has ceased at early stage of their evolution in the present study. In particular, we focus on the evolution of the relative contribution of the lobe and shell emission. We show that the shell will be dominant at most of the frequencies from radio up to gamma-ray soon after the jet is switched off and discuss the possibility for detecting the emission.

This paper is organized as follows. In Section 2, we introduce our dynamical model, which describes the evolution of the shell and cocoon, and explain how the energy distribution of the electrons residing in these regions and the spectra of the radiation they produce are evaluated. The obtained results are presented in Section 3. The summary and discussion of our results is given in Section 4. Throughout the paper, a Λ CDM cosmology with $H_0 = 71 \text{ km s}^{-1} \text{ Mpc}^{-1}$, $\Omega_M = 0.27$ and $\Omega_\Lambda = 0.73$ is adopted (Komatsu et al. 2009).

2. MODEL

Following the previous studies (Ito et al. 2011; Kino et al. 2013), we evaluate non-thermal emissions from cocoon and shell based on a simple analytical model that describes their dynamical expansion. The model is identical to that employed in the previous studies during the early phase when the jet is active. The only difference is that we properly take into account the evolution after the jet injection has ceased. In this section, we briefly review the employed model and explain the differences

from the previous studies.

First, let us summarize the basic assumptions in our model. (1) Regarding the ambient mass density, ρ_a , a power-law dependence on radius, r , with an index, α , is assumed, $\rho_a(r) = \rho_0(r/r_0)^{-\alpha}$. Here r_0 is the reference radius and ρ_0 is the mass density at the radius. In the present study, we adopt $\rho_0 = 0.1 m_p \text{ cm}^{-3}$, $r_0 = 1 \text{ kpc}$ and $\alpha = 1.5$ based on the values inferred from the observation of elliptical galaxies (e.g., Mulchaey & Zabludoff 1998; Mathews & Brighenti 2003; Fukazawa, Makishima, & Ohashi 2004; Fukazawa et al. 2006). Here m_p is the proton mass and $\rho_{0.1} = \rho_0/0.1 m_p$. The shape of the cocoon and shell are approximated as a sphere and neglect its elongation along the jet direction merely for simplicity. (2) We use the standard thin shell approximation (Ostriker & McKee 1988) and assume that most of the matter swept up by the bow shock is concentrated in a region of width δR , behind the shock which is thin compared with the radius of the shock, R .

Regarding the dynamics of expansion, we consider two phases depending on the age, t : (i) the early phase in which the jet injection is present ($t \leq t_j$) and (ii) the late phase in which the jet injection has ceased ($t > t_j$). Here t_j denotes the duration of the jet injection. As mentioned above, we use the same model used in the previous studies (Ito et al. 2011; Kino et al. 2013) in the early phase ($\dot{R} \equiv dR/dt \propto t^{-(2-\alpha)/(5-\alpha)}$). After the energy injection from the jet ceases, the cocoon will rapidly lose its energy due to adiabatic expansion and give away most of its energy into the shell within a dynamical timescale $\sim R/\dot{R}$. Hence, after the transition time $\sim R/\dot{R} \sim t_j$, cocoon pressure becomes dynamically unimportant, and the energy of the shell becomes dominant. Therefore, in the late phase, expansion of the bow shock is expected to akin to Sedov-Taylor expansion ($\dot{R} \propto t^{-(3-\alpha)/(5-\alpha)}$). Based on these considerations, we can approximately describe the two phases continuously by connecting the expansion velocity of the bow shock at $t = t_j$ as

$$\dot{R}(t) = \begin{cases} \dot{R}_0 \left(\frac{t}{t_j}\right)^{-(2-\alpha)/(5-\alpha)} & \text{for } 0 < t \leq t_j, \\ \dot{R}_0 \left(\frac{t}{t_j}\right)^{-(3-\alpha)/(5-\alpha)} & \text{for } t_j < t, \end{cases} \quad (1)$$

where

$$\dot{R}_0 = C \left(\frac{L_j}{\rho_0 r_0^\alpha}\right)^{1/(5-\alpha)} t_j^{(2-\alpha)/(5-\alpha)}. \quad (2)$$

Here L_j is the power of the jet and $C = 3/(5-\alpha)[(3-\alpha)(5-\alpha)^3(\hat{\gamma}_c-1)/\{4\pi(2\alpha^2+\alpha-18\hat{\gamma}_c\alpha+63\hat{\gamma}_c-28)\}]^{1/(5-\alpha)}$, where $\hat{\gamma}_c$ is the specific heat ratio of the plasma inside the cocoon. From the above equation, the radius of the bow shock is determined as $R(t) = \int_0^t \dot{R}(t') dt'$. In the present study, we assume $\hat{\gamma}_c = 4/3$, since plasma within the cocoon is expected to be relativistic.

Once the expansion velocity \dot{R} is obtained, the properties of the shell are determined in the same manner described in the previous study (Ito et al. 2011). We employ the non-relativistic Rankine-Hugoniot condition in the strong shock limit (Landau & Lifshitz 1959) and

evaluate the density and pressure in the shell as

$$\rho_s(t) = \frac{\hat{\gamma}_a + 1}{\hat{\gamma}_a - 1} \rho_a(R), \quad (3)$$

and

$$P_s(t) = \frac{2}{\hat{\gamma}_a + 1} \rho_a(R) \dot{R}(t)^2, \quad (4)$$

respectively, where $\hat{\gamma}_a$ is the specific heat ratio of the ambient medium. In the present study, we adopt $\hat{\gamma}_a = 5/3$ since the temperature of the ambient medium is non-relativistic. The shell width, δR , in which most of the mass swept up by the bow shock is contained is evaluated from the conservation of mass $\rho_s V_s = \int_0^R 4\pi r^2 \rho_a(r) dr$, where $V_s = 4\pi R^2 \delta R$ is the volume of the shell. Hence, the shell width is given by $\delta R = (\hat{\gamma}_a - 1)[(\hat{\gamma}_a + 1)(3 - \alpha)]^{-1} R$. As a result, the total internal energy of the shell, $E_s = P_s V_s / (\hat{\gamma}_a - 1)$, scales linearly with time as $E_s = f_1 L_j t \propto t$ for $t \leq t_j$ and gradually asymptotes to a constant value of $E_s = f_2 L_j t_j \propto t^0$ for $t \gg t_j$. Such a behaviour is naturally expected, because energy is continuously injected into the system from the jet with a constant rate when the jet is active, while there is no energy source after the jet activity ceases. Here f_1 and f_2 are the fractions of energy injected by the jet that are converted into the internal energy of the shell which are given by $f_1 = 18(\hat{\gamma}_c - 1)(5 - \alpha)(\hat{\gamma}_a + 1)^{-2}[2\alpha^2 + (1 - 18\hat{\gamma}_c)\alpha + 63\hat{\gamma}_c - 28]^{-1}$ and $f_2 = (3/2)^{3-\alpha} f_1$. For the values employed in the present study, ($\hat{\gamma}_c = 4/3$, $\hat{\gamma}_a = 5/3$ and $\alpha = 1.5$), $f_1 \sim 0.11$ and $f_2 \sim 0.21$ are obtained. Hence, the ratio of the internal energy of the shell to the total energy deposited in the system is roughly constant ($\sim 10 - 20\%$) throughout the evolution.

As described in the previous study (see §2.1 of Ito et al. 2011, for detail), for $t \leq t_j$, the pressure of the cocoon is directly obtained from the dynamical model and is given by

$$P_c(t) = f_p P_s(t), \quad (5)$$

where f_p is the ratio of the pressure of the cocoon to that of shell and is given as $f_p = (\hat{\gamma}_a + 1)(7 - 2\alpha)/[6(3 - \alpha)]$. For typical numbers, $\hat{\gamma}_a = 5/3$, $0 \leq \alpha \leq 2$, f_p depends on α only weakly and $f_p \sim 1$. This is expected, since the pressure of the shell and cocoon should be roughly equal (see e.g., Heinz et al. 1998). Since pressure balance is also expected for $t > t_j$, we assume that the ratio of the pressure is maintained and determine P_c from the same equation also in the later phase. Regarding the evolution of the radius of the cocoon, R_c , we assume $R_c = R$ for $t \leq t_j$ as in the previous studies. On the other hand, since the cocoon expands adiabatically, the cocoon radius satisfies $P_c V_c^{\hat{\gamma}_c} = \text{const}$, for $t > t_j$, where $V_c = 4\pi R_c^3/3$ is the volume of the cocoon. Hence, the evolution of the cocoon radius can be summarized as

$$R_c(t) = \begin{cases} R(t) & \text{for } 0 < t \leq t_j, \\ R(t_j) \left(\frac{P_c(t_j)}{P_c(t)} \right)^{1/3\hat{\gamma}_c} & \text{for } t_j < t. \end{cases} \quad (6)$$

As a result, cocoon expands slower than the shell in this phase and makes the region of the shocked shell wider. It is worth noting that similar behaviour is found in Reynolds & Begelman (1997). The total internal

energy deposited in the cocoon is evaluated from the obtained pressure and radius as $E_c = P_c V_c / (\hat{\gamma}_c - 1)$. For $t \leq t_j$, E_c scales linearly with time as $E_c = f_{\text{lobe},1} L_j t$ as in the case of the shell, where $f_{\text{lobe},1} = (5 - \alpha)(7 - 2\alpha)[2\alpha^2 + (1 - 18\hat{\gamma}_c)\alpha + 63\hat{\gamma}_c - 28]^{-1}$. At later time ($t > t_j$), the evolution of E_c asymptotes to $E_c = f_{\text{lobe},2} L_j t_j (t/t_j)^{-6(\hat{\gamma}_c-1)/[\hat{\gamma}_c(5-\alpha)]}$, where $f_{\text{lobe},2} = (2/3)^{\alpha(\hat{\gamma}_c-1)/\hat{\gamma}_c} f_{\text{lobe},1}$. For the values employed in the present study, ($\hat{\gamma}_c = 4/3$, $\hat{\gamma}_a = 5/3$ and $\alpha = 1.5$), $f_{\text{lobe},1} \sim 0.54$ and $f_{\text{lobe},2} \sim 0.46$ are obtained.

In determining energy distribution of non-thermal electrons, $N(\gamma_e, t)$, within the shell and lobe, we approximate each region as one-zone and solve the kinetic equation which takes into account the injection and cooling of particles given by

$$\frac{\partial N(\gamma_e, t)}{\partial t} = \frac{\partial}{\partial \gamma_e} [\dot{\gamma}_{\text{cool}}(\gamma_e, t) N(\gamma_e, t)] + Q(\gamma_e, t). \quad (7)$$

Here γ_e , $\dot{\gamma}_{\text{cool}} = -d\gamma_e/dt$, and Q are the Lorentz factor, the cooling rate via adiabatic and radiative losses, and the injection rate of accelerated electrons, respectively. The injection rate and the cooling rate are determined from the dynamical model in the same manner as described in the previous studies (Ito et al. 2011; Kino et al. 2013).⁵

Regarding the shell, we assume a continuous injection throughout the evolutions given by

$$Q(\gamma_e, t) = K(t) \gamma_e^{-p} \quad \text{for } \gamma_{\min} \leq \gamma_e \leq \gamma_{\max}(t). \quad (8)$$

Here γ_{\min} and γ_{\max} are the minimum and maximum Lorentz factors of the accelerated electrons, respectively. In the present study, we employ $\gamma_{\min} = 1$ and $p = 2$. In determining the maximum Lorentz factor, we assume that the acceleration is limited by cooling. As for the electron acceleration mechanism, we assume the well-known diffusive shock acceleration in which the acceleration rate can be written as $\dot{\gamma}_{\text{accel}} = 3eB\dot{R}^2/(20\xi m_e c^3)$ (e.g., Drury 1983). Here B is the magnetic field strength in the shell and ξ is the so-called ‘‘gyro-factor’’ which can be expressed as the ratio of the energy in ordered magnetic fields to that in turbulent ones ($\xi = 1$ corresponds the Bohm limit). Hence, the maximum Lorentz factor is given by the value where cooling rate, $\dot{\gamma}_{\text{cool}}(\gamma_e)$, and acceleration rate $\dot{\gamma}_{\text{accel}}$ become equal. The normalisation factor, K , is computed by assuming that a fraction, ϵ_e , of the shock-dissipated energy is carried by the non-thermal electrons. In our calculation, we assume constant energy injection rate throughout the evolution, and, for a given source age of $t = t_{\text{age}}$, the normalization factor at an arbitrary time ($t \leq t_{\text{age}}$), is determined from the equation: $\int_{\gamma_{\min}}^{\gamma_{\max}(t)} (\gamma_e - 1) m_e c^2 Q(\gamma_e, t) d\gamma_e = \epsilon_e E_s(t_{\text{age}})/t_{\text{age}}$. We choose $\xi = 1$ and $\epsilon_e = 0.01$ as fiducial values for the parameters that characterize the acceleration efficiencies based on the observations of supernova remnants (e.g., Dyer et al. 2001; Ellison et al. 2001; Bamba et al. 2003; Yamazaki et al. 2004; Stage et al. 2006; Tanaka et al. 2008), since the properties of the shock are similar to that of the bow shock considered here.

⁵ We note that the temporal evolutions of $\dot{\gamma}_{\text{cool}}$ and Q are taken into account in this paper and Kino et al. (2013), whereas they were neglected in Ito et al. (2011).

Considering the electron injection into the lobe, we assume continuous injection as in the case of the shell for $t \leq t_j$. In contrast, it is assumed that injection of the non-thermal electrons ceases for $t > t_j$, since the jet can no longer supply matter in this phase. Hence, the energy distribution of the electrons injected into the lobe is given as

$$Q_{\text{lobe}}(\gamma_e, t) = \begin{cases} K_{\text{lobe}}(t) \gamma_e^{-p_{\text{lobe}}} & (0 < t \leq t_j) \\ 0 & \text{for } \gamma_{\text{min,lobe}} \leq \gamma_e \leq \gamma_{\text{max,lobe}}, \\ & (t_j < t), \end{cases} \quad (9)$$

where $\gamma_{\text{min,lobe}}$ and $\gamma_{\text{max,lobe}}$ are the minimum and maximum Lorentz factors, respectively. The imposed values for the power-law index and minimum Lorentz factor are the same as those adopted for the shell ($p_{\text{lobe}} = 2$ and $\gamma_{\text{min,lobe}} = 1$). On the other hand, we use as fixed value $\gamma_{\text{max,lobe}} = 10^4$ for the maximum Lorentz factor. The employed value of $\gamma_{\text{max,lobe}}$ is based on multi-wavelength observations of FR II radio galaxies which suggest electrons within the lobe do not have Lorentz factor well beyond $\sim 10^4$ (Stawarz et al. 2007; Godfrey et al. 2009; Yaji et al. 2010). As shown in §3, it is noted, however, that the conclusion of the present study is insensitive to the assumed values of p_{lobe} , $\gamma_{\text{min,lobe}}$ and $\gamma_{\text{max,lobe}}$. In determining K_{lobe} , we assume that a fraction, $\epsilon_{e,\text{lobe}}$, of the energy deposited in the lobe is carried by non-thermal electrons and the energy injection rate of the non-thermal electrons are constant up to $t = t_j$: $\int_{\gamma_{\text{min,lobe}}}^{\gamma_{\text{max,lobe}}} (\gamma_e - 1) m_e c^2 Q(\gamma_e, t) d\gamma_e = \epsilon_{e,\text{lobe}} E_c(t_j)/t_j = f_{\text{lobe},1} L_j$. Although the value of $\epsilon_{e,\text{lobe}}$ is not constrained very well, we adopt $\epsilon_{e,\text{lobe}} = 1$ in the present study which is often assumed in previous studies (e.g., Stawarz et al. 2008; Ostorero et al. 2010; Ito et al. 2011).

Regarding energy loss rate, $\dot{\gamma}_{\text{cool}}$, we take into account radiative and adiabatic (expansion) losses. The adiabatic cooling is evaluated from the expansion of the system as $\dot{\gamma}_{\text{ad}} = (\dot{R}/R)\gamma_e$ for the shell and $\dot{\gamma}_{\text{ad}} = (\dot{R}_c/R_c)\gamma_e$ for the lobe, where $\dot{R}_c = dR_c/dt$. As for the radiative cooling, we consider the synchrotron radiation, $\dot{\gamma}_{\text{syn}}$, and the IC scattering $\dot{\gamma}_{\text{IC}}$.

The typical magnetic field strengths in elliptical galaxies and clusters of galaxies are inferred to be around few μG (e.g., Moss & Shukurov 1996; Vikhlinin, Markevitch, & Murray 2001; Clarke et al. 2001; Carilli & Taylor 2002; Schekochihin et al. 2005). Therefore, we adopt magnetic field strength of $B = 10\mu\text{G}$ in the shell for the calculation of synchrotron emission, since shock compression leads to amplification by a factor of $\sim 1 - 4$. On the other hand, magnetic field strength within the lobe, B_c , is determined under the assumption that a fraction ϵ_B , of the energy E_c is carried by the magnetic fields. In the present study we assume $\epsilon_B = 0.1$, a magnetic field strength factor of a few below the equipartition value which is in the range typically observed in radio galaxies (e.g., Isobe et al. 2002; Kataoka et al. 2003; Croston et al. 2004, 2005; Kataoka & Stawarz 2005).

Regarding the IC scattering, full Klein-Nishina (KN) cross section is taken into account (Blumenthal & Gould 1970) and, as a source of seed photon fields, we consider UV emission from the accretion disc, IR emission from the dusty torus, stellar emission in NIR from the host galaxy, synchrotron emission from the radio lobe

and cosmic microwave background (CMB). We modelled the spectra of the photons from the disc, torus and host galaxy with a black-body spectra peaking at frequencies given by $\nu_{\text{UV}} = 2.4 \times 10^{15}$ Hz, $\nu_{\text{IR}} = 1.0 \times 10^{13}$ Hz and $\nu_{\text{NIR}} = 1.0 \times 10^{14}$ Hz, respectively. As for the luminosities of the emissions, we adopt $L_{\text{UV}} = L_{\text{IR}} = 10^{45}$ erg s $^{-1}$ for the disc and torus emission (e.g., Elvis et al. 1994; Jiang et al. 2006), and $L_{\text{NIR}} = 10^{44}$ erg s $^{-1}$ for the host galaxy emission (e.g., de Ruiter et al. 2005). CMB is given by a black-body that has peak frequency and energy density given by $\nu_{\text{CMB}} = 1.6 \times 10^{11}(1+z)$ Hz and $U_{\text{CMB}} \approx 4.2 \times 10^{-13}(1+z)^4$ erg cm $^{-3}$, respectively, where z is the cosmological redshift of the source. The spectrum of the seed photon field of the synchrotron emission from the lobe is obtained in our calculation self-consistently. The IC cooling is determined by the given spectra and source size as in the previous study (for detail, see §2.2 and §4.1 of Ito et al. 2011).

The energy distribution of non-thermal electrons, $N(\gamma_e, t)$, is obtained by putting the evaluated injection rate, $Q(\gamma_e, t)$, and the cooling rate, $\dot{\gamma}_{\text{cool}}(\gamma_e, t)$, in Equation (7). The spectra of the synchrotron and IC emission are self-consistently calculated from the obtained energy distribution (for detail, see §2.3 and §4.1 of Ito et al. 2011).

As shown in the previous studies, thermal emission is also an important ingredient when considering the shell emission (e.g., Heinz et al. 1998; Kaiser & Alexander 1999; Reynolds et al. 2001; Zanni et al. 2003; Bordas et al. 2011). Therefore, we also calculate the thermal bremsstrahlung emission from the shell in the present study. Under the assumption that most of the shock dissipated energy is converted into that of the thermal electrons, the luminosity is estimated as $L_{\nu,\text{brem}} = 2^5 \pi e^6 / (3m_e c^3) [2\pi / (3k_B m_e)]^{1/2} n_e^2 T^{-1/2} e^{-h\nu/k_B T} \bar{g}_{ff}$, where k_B is the Boltzmann constant, and $n_e = \rho_s/m_p$, and $T = P_s/2n_e k_B$ are the number density and temperature of the thermal electrons within the shell, respectively. Here \bar{g}_{ff} is the Gaunt factor (Rybicki & Lightman 1979) and is set to be unity merely for simplicity.

3. RESULTS

In this section, we show the time evolutions of the energy distribution of non-thermal electrons and the resulting emission. As a fiducial case we focus on sources with jet power of $L_j = 10^{45}$ erg s $^{-1}$. Since our aim is to explore the evolution of short-lived sources in which the energy injection into the lobe have stopped in the early stage of their evolution, we set the duration of energy injection as $t_j = 10^5$ yr. The chosen value of the age is around the upper end of the estimated age of the compact radio source (e.g., Murgia 2003; Polatidis & Conway 2003). The overall linear size at $t = t_j$ is $2R(t_j) \sim 0.86 \rho_{0.1}^{-2/7} L_{45}^{2/7} t_{j,5}^{6/7}$ kpc, where $L_{45} = L_j/10^{45}$ erg s $^{-1}$ and $t_{j,5} = t_j/10^5$ yr.

It is noted that, since spherical symmetry is assumed, the source size and age correspondence predicted in our model show relatively large discrepancy from those inferred from the observations (e.g., Owsianik et al. 1999; Taylor et al. 2000; Conway 2002). The actual source geometry is elongated along the jet axis, and, for a given source age, their linear sizes along the jet direction and

transverse direction are larger and smaller by a factor \sim a few, respectively. It is emphasized, however, that the discrepancy does not have significant effect on the essential features of our results, since large axial ratio is rarely observed. Moreover, the axial ratio is reduced after the jet activity ceases ($t > t_j$), i.e. the phase that we mainly focus on this study, since the thrust from the jet which causes the elongation is no longer present. Therefore, we can consider that the results obtained in the present study at a given age t apply to the sources whose linear extension is larger than $R(t)$ within a factor of few.

3.1. Evolution of Non-thermal Electrons

In Figure 1 we display the energy distribution of non-thermal electrons within the lobe (*left panel*) and shell (*right panel*) for different source ages ($t = 10^5, 1.1 \times 10^5, 2 \times 10^5, 5 \times 10^5$ and 10^6 yr). When the jet is active ($t \leq t_j$), the non-thermal electrons are continuously supplied in the shell and lobe. In this initial phase, the energy distributions of electrons within the lobe and shell show a broken power-law shape. The break is located at the energy where the cooling time of the electrons becomes roughly equal to the dynamical time ($t \sim t_{\text{cool}}(\gamma_e)$). Below the break energy, the electron energy distribution maintains the form of the injected energy spectrum which is roughly given by $N(\gamma_e) \sim Q(\gamma_e)t \propto \gamma_e^{-2}$, since the cooling effect is negligible at these energies. Above the break energy, the energy distribution is modified by the cooling loss and can be roughly approximated as $N(\gamma_e) \sim Q(\gamma_e)t_{\text{cool}}(\gamma_e)$ with a sharp cut-off at the injected maximum energy (γ_{max} and $\gamma_{\text{max,lobe}}$, for the shell and lobe, respectively). While for the shell the dominant radiative cooling is provided by the IC scattering off the disc and torus photons, synchrotron cooling is slightly larger than the IC cooling for the lobe. Since the cooling is more rapid in the lobe, the break energy is lower than that of the shell (see Ito et al. 2011, for more detail).

After the jet activity has ceased ($t > t_j$), the evolution of electron energy distribution differs largely between the shell and lobe. Regarding the shell, the evolution does not show large change from that at the early phase ($t \leq t_j$). The electron energy distribution can be roughly described by a broken power-law shape. The radiative loss is mainly dominated by the IC scattering of the torus photons. Since the energy density of the photon decreases with the source size $U_{\text{ph}} \propto R^{-2}$, the break energy gradually increases with the age.

On the other hand, due to the cessation of the electron injection ($Q(\gamma_e) = 0$), the evolution of the energy distribution of the electrons in the lobe changes drastically from that at the early phase ($t \leq t_j$). Since fresh electrons are no longer supplied, population of electrons with energy above the break energy determined at $t = t_j$ rapidly decreases because of the cooling loss. The cooling proceeds predominantly through synchrotron emission and the corresponding break energy is found at

$$\begin{aligned} \gamma_{\text{br,lobe}} &\approx 3m_e c / (4\sigma_T U_{\text{B,lobe}} t) \\ &\sim 4.8 \times 10^2 \epsilon_{\text{B,-1}} \rho_{0.1}^{-6/7} L_{45}^{-1/7} t_{j,5}^{4/7}, \end{aligned} \quad (10)$$

where $U_{\text{B,lobe}} = B_{\text{lobe}}^2 / 8\pi$, $\epsilon_{\text{B,-1}} = \epsilon_{\text{B}} / 0.1$ and $t_{j,5} = t_j / 10^5 \text{ yr}$. The rapid depletion continues until $t \sim 2t_j$ at which all the high energy electrons ($\gamma_e \gtrsim \gamma_{\text{br,lobe}}$) are

cooled. Thereafter, electrons gradually cool mainly due to adiabatic loss ($\gamma_e \propto R_c^{-1} \propto t^{-3/7}$). These features are clearly seen in Figure 1.

3.2. Evolution of Broadband Emission

In Figure 2, we show the corresponding evolution of the total photon fluxes, νf_ν , from the shell (solid lines) and lobe (dashed lines) for a source located at the redshift of $z = 1$. Together with the total photon fluxes, the contributions from the synchrotron emission, and IC scattering of various seed photons are displayed in Figure 3 for a source with $t = 10^5$ yr and 10^6 yr. As mentioned in the previous section, contribution from the thermal bremsstrahlung emission is also considered for the shell emission. Attenuations due to synchrotron self-absorption (SSA) and pair production due to photon-photon interaction are also taken into account in the spectra. The absorption coefficient for SSA within the lobe, $\alpha_{\text{lobe},\nu}$, and shell $\alpha_{\text{s},\nu}$ are determined independently from the magnetic field strength and electron energy distribution within these regions following Rybicki & Lightman (1979). The spectra of the shell and lobe below the frequency which satisfy $\alpha_{\text{s},\nu} R = 1$ and $\alpha_{\text{lobe},\nu} R_c = 1$ (optically thick), respectively, are described as $f_\nu \propto \nu^{5/2}$. Note that the absorption in the lobe is much stronger than that of the shell since the number of non-thermal electrons and magnetic field strength within the lobe is larger than those of the shell. Gamma-rays above energy $\gtrsim 100$ GeV are subject to pair production due to photon-photon interaction with optical-infrared background radiation. Here we used the model of Franceschini et al. (2008) for the background radiation and evaluated the attenuated photon fluxes shown in Figures 2 and 3. We also plot the unattenuated gamma-ray spectra in Figure 3 (dotted line).

3.2.1. Lobe emission

Regarding lobe emission, synchrotron and IC components produce prominent emission extending from radio up to $h\nu \sim 10$ GeV when the jet is active ($t \leq t_j$). Their overall luminosities are roughly comparable and proportional to energy injection rate into the non-thermal electrons ($\nu L_\nu \propto \epsilon_{e,\text{lobe}} L_j$). This is simply because the energy injected into the non-thermal electrons $\epsilon_{e,\text{lobe}} L_j$ is immediately converted into the radiation.

After the jet activity ceases ($t > t_j$), due to the absence of particle injection, radiative cooling leads to rapid depletion of high energy electrons $\gamma_e > \gamma_{\text{br,lobe}}$ within the lobe. As mentioned earlier, this rapid decrease continues until all the electrons above the break energy radiate away most of their energy $t \sim 2t_j$ (Figure. 1). As a result, the high energy cut-off frequency rapidly shifts to the lower energies and the overall emission fades out quite rapidly, as seen in Figure 2. It is worth noting that this passive feature of the lobe emission is consistent with the previous theoretical studies (Komissarov & Gubanov 1994; Nath 2010; Mocz et al. 2011) and provides a natural explanation for the reason why dying radio sources, so-called faders, are rarely found in the observations (Kunert-Bajraszewska et al. 2005, 2006; Orienti et al. 2010). After this passive phase ($t \gtrsim 2t_j$), although relatively slow, the emission continues to fade predominantly through adiabatic cooling. It is stressed

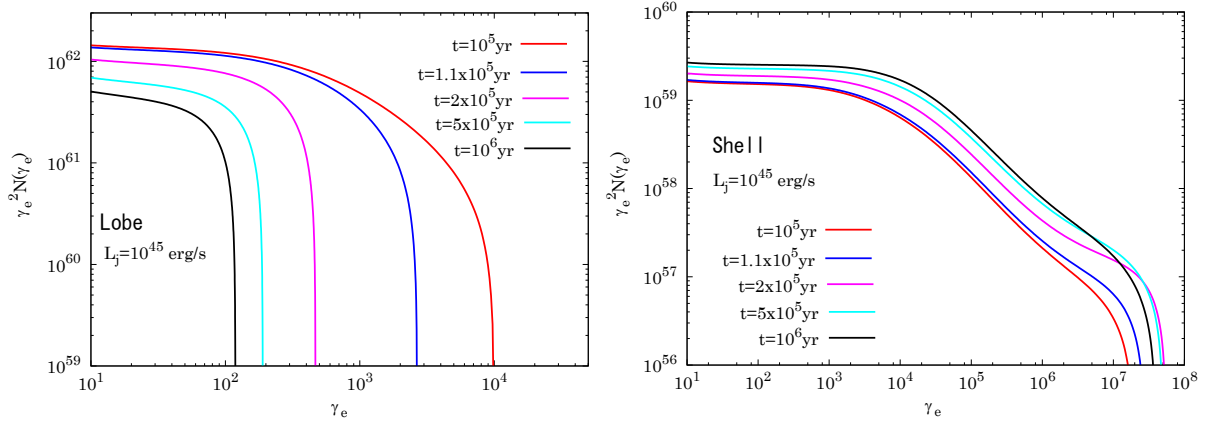


Figure 1. Energy distributions of non-thermal electrons within the shell (*right panel*) and lobe (*left panel*) for source with jet power of $L_j = 10^{45} \text{ erg s}^{-1}$ and injection duration of $t_j = 10^5 \text{ yr}$. The various lines display the cases for sources with ages of 10^5 (red line), 1.1×10^5 (blue line), 2×10^5 (purple line), 5×10^5 (light blue line) and 10^6 yr (black line).

that the evolution at the fading phase ($t > t_j$) is insensitive to the assumed value of $\gamma_{\text{max,lobe}}$ or the assumptions on the seed photon fields, since $\gamma_{\text{br,lobe}}$ does not depend on these assumptions.

3.2.2. Shell emission

Regarding emission from the shell, as in the case of the lobe, the overall luminosity of the non-thermal emission is proportional to the jet power and the energy fraction of the non-thermal electrons ($\nu L_\nu \propto \epsilon_e L_j$) when the jet is active $t \leq t_j$. However, much fainter emission is produced in the shell, since smaller energy fraction is assumed ($\epsilon_e \ll \epsilon_{e,\text{lobe}}$). Unlike in the case of the lobe, IC emission is brighter than the synchrotron emission, since the energy density of magnetic field, $U_B = B^2/8\pi$ is much smaller than that of the seed photons. ($U_B \ll U_{\text{ph}}$). Since the maximum energy of the electron is larger than that of the lobe ($\gamma_{\text{max}} \gg \gamma_{\text{max,lobe}}$), the overall spectrum extends up to higher frequencies. The high energy cut-off is observed at $h\nu \sim 1 - 10 \text{ TeV}$, and at this high energy range the spectrum is modified by the attenuation due to pair production (Figure 3).

As mentioned in §3.1, the evolution of non-thermal electrons at the later phase ($t > t_j$) does not show large change from the initial phase ($t \leq t_j$). The overall luminosity continues to be dominated by the IC emission. As in the case of the lobe, the emission from the shell begins to fade in this phase. On the other hand, however, their cut-off frequency $h\nu \sim 1 - 10 \text{ TeV}$ remains nearly unchanged and the decrease in the luminosity proceeds much more slowly (Figure 2). As in the initial phase, the overall luminosity is proportional to the energy injection rate into the non-thermal electrons ($\nu L_\nu \propto \epsilon_e L_j t_j/t$). Hence, after the jet injection has ceased the luminosity gradually decreases with age as $\nu L_\nu \propto t^{-1}$, if the energy fraction of electrons ϵ_e does not vary with time. This large difference in the behaviour of luminosity evolution between the lobe and shell is mainly due to the fact that the fresh electrons that are accelerated at the bow shock are continuously supplied into the shell even after the jet cessation.

In contrast with the non-thermal emission, the thermal bremsstrahlung emission from the shell has a rel-

atively weak dependence on the jet power and has a strong dependence on the ambient medium. The emission produces a bump in the spectra at X-ray frequencies ($h\nu \sim 1 - 100 \text{ keV}$) with peak frequency given as $h\nu \sim k_B T \propto \dot{R}(t)^2$ and dominates over the non-thermal emission as seen in the Figures. 2 and 3.

3.2.3. Comparison between lobe and shell

Finally, let us compare the emission from the lobe and shell. In the initial phase when the jet is active ($t \leq t_j$), the result does not vary from those obtained in the previous studies (Ito et al. 2011; Kino et al. 2013), since the same set up is used for the calculation. The lobe emission dominates over the shell emission up to their cut-off frequency ($h\nu \sim 10 \text{ GeV}$). At higher energies, however, the shell emission becomes dominant up to $h\nu \sim 1 - 10 \text{ TeV}$.

On the other hand, soon after the cessation of the jet activity ($t > t_j$), emission from the shell becomes dominant at most of the frequencies due to the rapid decrease of the lobe luminosity. For example, the emission from the shell overwhelms that of the lobe at frequencies $\gtrsim 10^7 \text{ Hz}$ for sources with age of $t \gtrsim 10^6 \text{ yr}$ (see Figure 3). As a result, dead radio sources eventually become dominated by the shell emission even at the radio frequencies. This shell-dominated phase is expected to continue up to the age where the expansion velocity becomes subsonic, since particle acceleration is unlikely to take place thereafter. As discussed in next section, the corresponding age can be as large as $\gtrsim 10^7 \text{ yr}$. Until then, luminosity of the shell gradually decreases as $\propto t^{-1}$. It is noted that the candidate of dying radio sources found in the observations (Kunert-Bajraszewska et al. 2005, 2006; Orienti et al. 2010) should be in passive phase ($t_j < t < 2t_j$) which means that the lobe emission has started to fade, but still dominates the emission at radio wavelengths.

4. SUMMARY AND DISCUSSIONS

In the present study, we have explored the evolution of the emission from the lobe and shell of radio sources which have ceased their jet activity in early stage of their evolution ($t_j \lesssim 10^5 \text{ yr}$). It is shown that the lobe emission rapidly fades after the jet injection has been stopped ($t > t_j$) due to the absence of particle supply from the

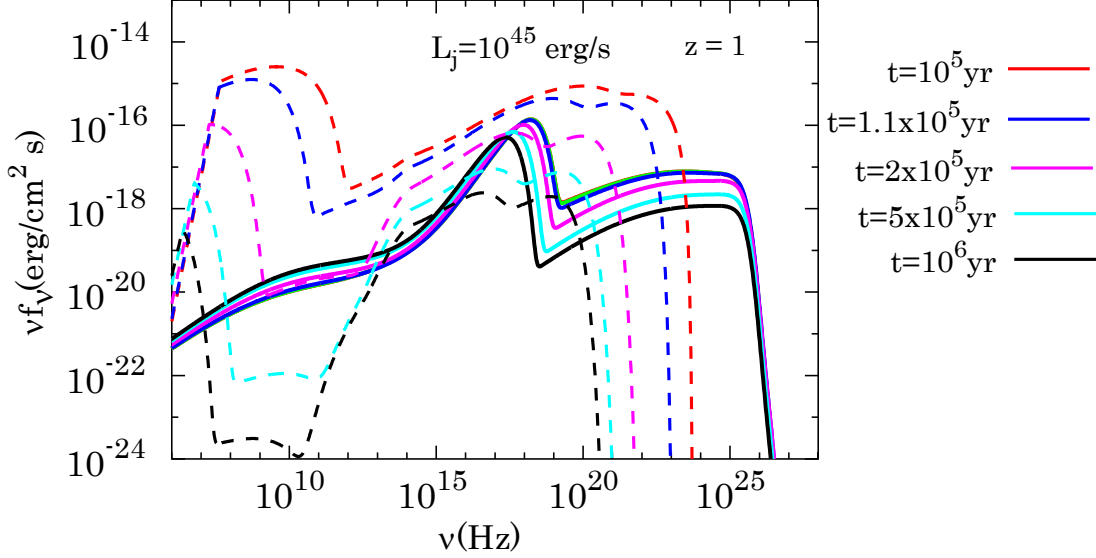


Figure 2. Broadband spectrum of source with a jet power of $L_j = 10^{45} \text{ erg s}^{-1}$ that located at the redshift of $z = 1$, and an injection time $t_j = 10^5 \text{ yr}$. The dashed lines and solid lines display the emission produced within the lobe and shell, respectively, for sources with age of 10^5 yr (red line), $1.1 \times 10^5 \text{ yr}$ (blue line), $2 \times 10^5 \text{ yr}$ (purple line), $5 \times 10^5 \text{ yr}$ (light blue line) and 10^6 yr (black).

jet. On the other hand, shell emission only shows gradual decay even after the jet activity has stopped since supply of electrons from the bow shock is maintained. Therefore, although faint, emission from the dying radio sources eventually becomes shell dominated at wide range of frequencies from radio up to gamma-ray.

Our results suggest that shell emission is essential for studying the nature of dead radio sources. Shell emission may be detectable for exceptionally high power sources ($L_j \gtrsim 10^{46} \text{ erg s}^{-1}$; e.g., Ito et al. 2008) that are located nearby ($z \lesssim 0.2$). On the other hand, for typical sources ($L_j \sim 10^{45} \text{ erg s}^{-1}$) located at redshift of $z \sim 1$, (a typical value for compact radio sources; e.g., O’Dea 1998), the emission is below the thresholds of the current instruments at any frequencies (see Figure. 3). This provides a natural explanation why such a shell emission has not been reported so far. Regarding the future missions, SKA telescope is capable of detecting the emission in the radio band. As shown in Figure. 3, the detection is marginal for SKA phase 1 (the emission slightly exceeds 3σ detection limit for an integration time of 10 hours with conservative values of $\epsilon_e = 0.01$ and $L_j = 10^{45} \text{ erg s}^{-1}$). It is noted that the emission is roughly linearly proportional to the acceleration efficiency ϵ_e and jet power L_j . Since these values inevitably have dispersion from source to source, we can expect a certain fraction of sources to be well above the detection limit. Moreover, in the phase 2 (SKA2), the sensitivity is expected improve by an order of magnitude. Hence, SKA will be a powerful tool to reveal the population of dead radio sources which are dominated by the shell emission.

In order to confirm that the emission comes from the shell rather than lobe, spatial angular resolution of the observation is important. If the emission is indeed produced in the shell, we expect to see limb brightening features (Heinz et al. 1998; Bordas et al. 2011). The emission will appear as an extended source with a total angular size given as $\sim 2(2R/5 \text{ kpc})(D_A/1 \text{ Gpc})^{-1} \text{ arcsec}$,

where D_A is the angular diameter ($D_A \sim 1.6 \text{ Gpc}$ for $z = 1$). Hence, high spacial resolution ($\sim 0.1 \text{ arcsec}$) provided by SKA can detect such a surface brightness distribution.

The shell emission dominated phase is expected to persist until the expansion velocity $\dot{R}(t)$ becomes subsonic, since, thereafter, strong shock will no longer be present. The sound speed in ambient gas is given as $c_s = [\gamma_a k_B T_a / (\mu m_p)]^{1/2}$, where T_a and $\mu = 0.6$ are the temperature and mean molecular weight of the ambient gas, respectively. Then the age when the source becomes subsonic ($\dot{R}/c_s = 1$) can be estimated as $t_s \approx 8.4 \times 10^6 (L_{45}/\rho_{0.1})^{2/3} t_{j,5}^{4/3} T_{\text{keV}}^{-7/6} \text{ yr}$, where $T_{\text{keV}} = k_B T_a / 1 \text{ keV}$. From the above equation, it is confirmed that the duration of shell dominated phase is much longer than that of the lobe dominated phase ($t_s - t_j \gg t_j$). Therefore, if large fraction of young radio sources die before becoming classical extended radio galaxies ($t \sim 10^7 - 10^8 \text{ yr}$) as indicated in previous studies (Alexander 2000; Marecki et al. 2003; Gugliucci et al. 2005; Orienti & Dallacasa 2010; Orienti et al. 2010; Kunert-Bajraszewska et al. 2010), our results predict the existence of a large population of undetected shell dominated sources residing in the universe. We expect that future survey by SKA will enable us to perform systematic study of these sources and quantify the fraction of dying sources through the detection of their shell emission. These observations will provide an important constraint on the evolution of radio sources.

Lastly, let us comment on the radio sources which stop their jet activity after becoming classical extended radio lobes (Fanaroff & Riley 1974). Although we focused on the sources which die at an early stage of their evolution ($\lesssim 10^5 \text{ yr}$), qualitatively similar results are expected for such sources. As shown in the present study, their lobe emissions fade rapidly and eventually become shell dominated. Actually, candidates of dead classical radio galaxies that are in the lobe fading phase have been found in

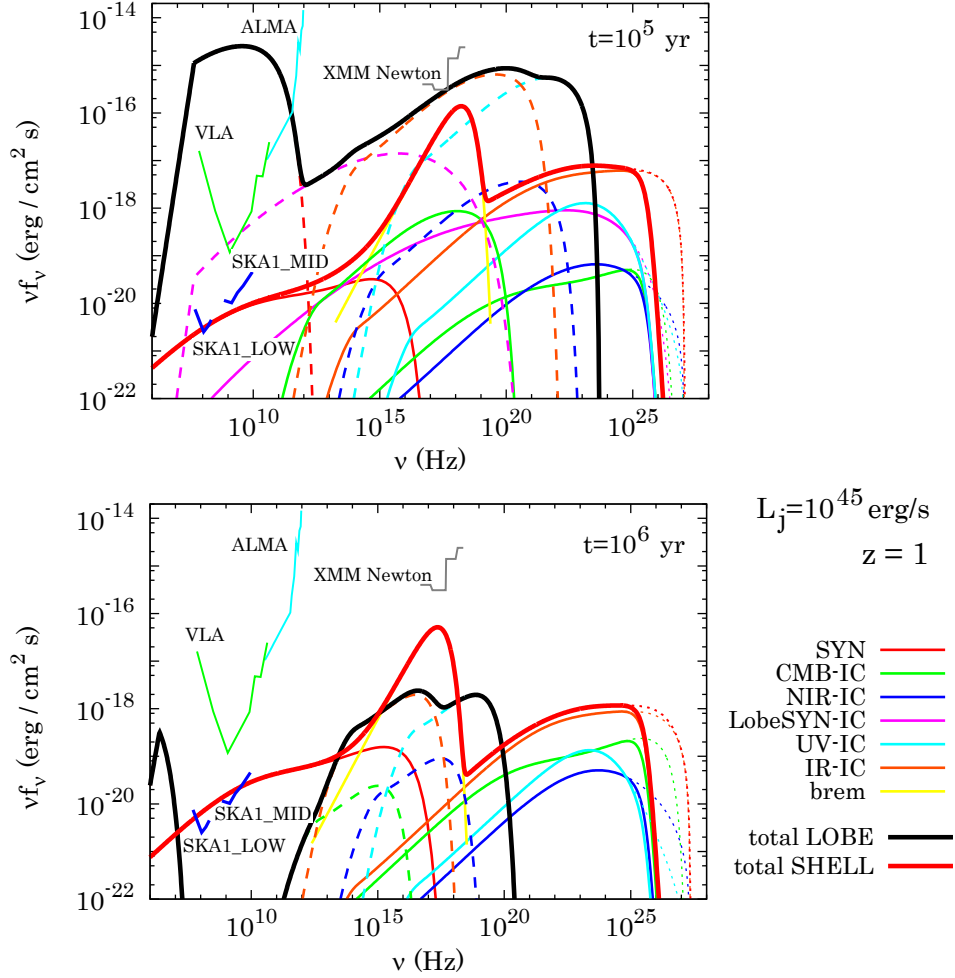


Figure 3. Broadband spectrum of source with a jet power of $L_j = 10^{45} \text{ erg s}^{-1}$ that is located at the redshift of $z = 1$. The top and bottom panels display the spectra for sources with ages of 10^5 and 10^6 yr, respectively. The thick black and thick red lines show the total flux from the shell and lobe, respectively. The various thin dashed and thin solid lines show the contributions to the total emission produced in the lobe and shell, respectively, from the synchrotron emission (red line) and the IC scattering of UV disk photons (light blue line), IR torus photons (orange line), NIR host galaxy photons (blue line), CMB photons (green line) and lobe synchrotron photons (purple line). The contribution from the thermal bremsstrahlung emission is also shown for the shell (yellow line). The dotted lines show the case when the attenuation due to pair production is neglected. Also shown are the sensitivities of the XMM-Newton, ALMA, Jansky VLA and SKA1 (SKA1_MID and SKA1_LOW). The assumed integration times for XMM-Newton, Jansky VLA and ALMA are 100 ks, 4 and 10 hours, respectively. The sensitivity of ALMA is calculated by using the ALMA Sensitivity Calculator (<https://almascience.eso.org/proposing/sensitivity-calculator>). As for SKA, we display 3σ detection limit for an integration time of 10 hours which is calculated based on the Appendix of Prandoni & Seymour (2014).

the observations (e.g., Murgia et al. 2011; Hurley-Walker et al. 2015). Therefore, we also expect to find the scaled up version of the compact shell dominated sources considered in the present study. Such sources are also very interesting and detectable by the SKA. Provided that the observed numbers of compact ($t \lesssim 10^5$ yr) and well extended radio source ($t \sim 10^7 - 10^8$ yr) are comparable (Fanti et al. 1995), the detection rate of such sources are expected to be roughly comparable to those end their jet activity at an early stage of their evolution ($\lesssim 10^5$ yr).

We are grateful to the anonymous referee for constructive comments which improved the clarity of the paper. N.K. acknowledges the financial support of Grant-in-Aid for Young Scientists (B:25800099). This work was partly supported by the Grant-in-Aid for Young Scien-

tists (B: 26800159) from the Ministry of Education, Culture, Sports, Science and Technology, Japan. Part of this work was done with the contribution of the Italian Ministry of Foreign Affairs and Research for the collaboration project between Italy and Japan.

REFERENCES

- Abdo, A. A., Ackermann, M., Ajello, M., et al. 2010, *Science*, 328, 725
- Alexander, P. 2000, *MNRAS*, 319, 8
- Bamba, A., Yamazaki, R., Ueno, M., & Koyama, K. 2003, *ApJ*, 589, 827
- Begelman, M. C., & Cioffi, D. F. 1989, *ApJ*, 345, 21
- Begelman, M. C., Blandford, R. D., & Rees, M. J. 1984, *Reviews of Modern Physics*, 56, 255
- Berezhko, E. G. 2008, *ApJ*, 684, L69

- Blumenthal, G. R., & Gould, R. J. 1970, *Reviews of Modern Physics*, 42, 237
- Bordas, P., Bosch-Ramon, V., & Perucho, M. 2011, *MNRAS*, 8
- Carilli, C. L., Perley, R. A., & Dreher, J. H. 1988, *ApJ*, 334, L73
- Carilli, C. L., Perley, R. A., & Harris, D. E. 1994, *MNRAS*, 270, 173
- Carilli, C. L., & Taylor, G. B. 2002, *ARA&A*, 40, 319
- Clarke, T. E., Kronberg, P. P., & Böhringer, H. 2001, *ApJ*, 547, L111
- Conway, J. E. 2002, *NewAR*, 46, 263
- Croston, J. H., Birkinshaw, M., Hardcastle, M. J., & Worrall, D. M. 2004, *MNRAS*, 353, 879
- Croston, J. L., Hardcastle, M. H., Harris, D. E., Besole, E., Birkinshaw, M., & Worrall, D. M. 2005, *ApJ*, 626, 733
- Croston, J. H., Kraft, R. P., & Hardcastle, M. J. 2007, *ApJ*, 660, 191
- Croston, J. H., et al. 2009, *MNRAS*, 395, 1999
- Drury, L. O. 1983, *Reports on Progress in Physics*, 46, 973
- Dyer, K. K., Reynolds, S. P., Borkowski, K. J., Allen, G. E., & Petre, R. 2001, *ApJ*, 551, 439
- Ellison, D. C., Slane, P., & Gaensler, B. M. 2001, *ApJ*, 563, 191
- Elvis, M., et al. 1994, *ApJS*, 95, 1
- Fanaroff, B. L., & Riley, J. M. 1974, *MNRAS*, 167, 31P
- Fanti, C., Fanti, R., Dallacasa, D., et al. 1995, *A&A*, 302, 317
- Franceschini, A., Rodighiero, G., & Vaccari, M. 2008, *A&A*, 487, 837
- Fujita, Y., Kohri, K., Yamazaki, R., & Kino, M. 2007, *ApJ*, 663, L61
- Fukazawa, Y., Botoya-Nones, J. G., Pu, J., Ohto, A., & Kawano, N. 2006, *ApJ*, 636, 698
- Fukazawa, Y., Makishima, K., & Ohashi, T. 2004, *PASJ*, 56, 965
- Godfrey, L. E. H., et al. 2009, *ApJ*, 695, 707
- Gugliucci, N. E., Taylor, G. B., Peck, A. B., & Giroletti, M. 2005, *ApJ*, 622, 136
- Hardcastle, M. J., Birkinshaw, M., Cameron, R. A., et al. 2002, *ApJ*, 581, 948
- Heinz, S., Reynolds, C. S., & Begelman, M. C. 1998, *ApJ*, 501, 126
- Hurley-Walker, N., Johnston-Hollitt, M., Ekers, R., et al. 2015, *MNRAS*, 447, 2468
- Isobe, N., Tashiro, M., Makishima, K., Iyomoto, N., Suzuki, M., Murakami, M. M., Mori, M., & Abe, K. 2002, *ApJ*, 580, L111
- Ito, H., Kino, M., Kawakatu, N., Isobe, N., & Yamada, S. 2008, *ApJ*, 685, 828
- Ito, H., Kino, M., Kawakatu, N., & Yamada, S. 2011, *ApJ*, 730, 120
- Jetha, N. N., Hardcastle, M. J., Ponman, T. J., & Sakellou, I. 2008, *MNRAS*, 391, 1052
- Jiang, L., et al. 2006, *AJ*, 132, 2127
- Kaiser, C. R., & Alexander, P. 1999, *MNRAS*, 305, 707
- Kataoka, J., Leahy, J. P., Edwards, P. G., et al. 2003, *A&A*, 410, 833
- Kataoka, J., & Stawarz, L. 2005, *ApJ*, 622, 797
- Kino, M., Ito, H., Kawakatu, N., & Orienti, M. 2013, *ApJ*, 764, 134
- Komatsu, E., Dunkley, J., Nolte, M. R., et al. 2009, *ApJS*, 180, 330
- Komissarov, S. S., & Gubanov, A. G. 1994, *A&A*, 285, 27
- Kraft, R. P., Vázquez, S. E., Forman, W. R., et al. 2003, *ApJ*, 592, 129
- Kunert-Bajraszewska, M., Gawroński, M. P., Labiano, A., & Siemiginowska, A. 2010, *MNRAS*, 408, 2261
- Kunert-Bajraszewska, M., Marecki, A., Thomasson, P., & Spencer, R. E. 2005, *A&A*, 440, 93
- Kunert-Bajraszewska, M., Marecki, A., & Thomasson, P. 2006, *A&A*, 450, 945
- Landau, L., & Lifshitz, F. M. 1959, *Fluid Mechanics* (London: Pergamon)
- Marecki, A., Spencer, R. E., & Kunert, M. 2003, *PASA*, 20, 46
- Mathews, W. G., & Brighenti, F. 2003, *ARA&A*, 41, 191
- Mocz, P., Fabian, A. C., & Blundell, K. M. 2011, *MNRAS*, 413, 1107
- Moss, D., & Shukurov, A. 1996, *MNRAS*, 279, 229
- Mulchaey, J. S., & Zabludoff, A. I. 1998, *ApJ*, 496, 73
- Murgia, M. 2003, *PASA*, 20, 19
- Murgia, M., Parma, P., Mack, K.-H., et al. 2011, *A&A*, 526, AA148
- Nath, B. B. 2010, *MNRAS*, 407, 1998
- O'Dea, C. P. 1998, *PASP*, 110, 493
- Orienti, M., & Dallacasa, D. 2010, 10th European VLBI Network Symposium and EVN Users Meeting: VLBI and the New Generation of Radio Arrays,
- Orienti, M., Murgia, M., & Dallacasa, D. 2010, *MNRAS*, 402, 1892
- Ostorero, L., et al. 2010, *ApJ*, 715, 1071
- Ostriker, J. P., & McKee, C. F. 1988, *Reviews of Modern Physics*, 60, 1
- Owsianik, I., Conway, J. E., & Polatidis, A. G. 1999, *NewAR*, 43, 669
- Perucho, M., Quilis, V., & Martí, J.-M. 2011, *ApJ*, 743, 42
- Polatidis, A. G., & Conway, J. E. 2003, *PASA*, 20, 69
- Prandoni, I., & Seymour, N. 2014, arXiv:1412.6512
- Reynolds, C. S., & Begelman, M. C. 1997, *ApJ*, 487, L135
- Reynolds, C. S., Heinz, S., & Begelman, M. C. 2001, *ApJ*, 549, L179
- Reynolds, C. S., Heinz, S., & Begelman, M. C. 2002, *MNRAS*, 332, 271
- de Ruiter, H. R., Parma, P., Capetti, A., Fanti, R., Morganti, R., & Santantonio, L. 2005, *A&A*, 439, 487
- Rybicki, G. B., & Lightman, A. P. 1979, *New York, Wiley-Interscience*, 1979. 393 p.,
- Schekochihin, A. A., Cowley, S. C., Kulsrud, R. M., Hammett, G. W., & Sharma, P. 2005, *ApJ*, 629, 139
- Stage, M. D., Allen, G. E., Houck, J. C., & Davis, J. E. 2006, *Nature Physics*, 2, 614
- Stawarz, L., Cheung, C. C., Harris, D. E., & Ostrowski, M. 2007, *ApJ*, 662, 213
- Stawarz, L., Ostorero, L., Begelman, M. C., Moderski, R., Kataoka, J., & Wagner, S. 2008, *ApJ*, 680, 911
- Tanaka, T., et al. 2008, *ApJ*, 685, 988
- Taylor, G. B., Marr, J. M., Pearson, T. J., & Readhead, A. C. S. 2000, *ApJ*, 541, 112
- Vikhlinin, A., Markevitch, M., & Murray, S. S. 2001, *ApJ*, 549, L47
- Wilson, A. S., Young, A. J., & Shopbell, P. L. 2000, *ApJ*, 544, L27
- Wilson, A. S., Smith, D. A., & Young, A. J. 2006, *ApJ*, 644, L9
- Yamazaki, R., Yoshida, T., Terasawa, T., Bamba, A., & Koyama, K. 2004, *A&A*, 416, 595
- Yaji, Y., Tashiro, M. S., Isobe, N., Kino, M., Asada, K., Nagai, H., Koyama, S., & Kusunose, M. 2010, *ApJ*, 714, 37
- Zanni, C., Bodo, G., Rossi, P., Massaglia, S., Durbala, A., & Ferrari, A. 2003, *A&A*, 402, 949